PCCP

Accepted Manuscript

ROYAL SOCIETY OF CHEMISTRY

www.rsc.org/pccp

Journal Name

RSCPublishing

COMMUNICATION

A theoretical study of the L_3 pre-edge XAS in Cu(II) complexes

Cite this: DOI: 10.1039/xoxxoooooox

G. Mangione,[a] M. Sambi,[a] M. V. Nardi[b,c] and M. Casarin*[a]

Received ooth January 2012,
Accepted ooth January 2012

DOI: 10.1039/xoxxoooooox

www.rsc.org/

$L_{2,3}$ spectra of Cu(II) complexes have been simulated by means of time dependent DFT. Besides the agreement between theory and experiment, the adopted approach provided further insights into the use of the Cu(II) L_3-edge intensity and position to investigate the Cu–ligand symmetry-restricted covalency and the ligand-field strength.

X-ray absorption spectroscopy (XAS) is unanimously recognized as a tool able to provide a site selective probe of the molecular unoccupied electronic structure.[1] XAS implies the excitation of core electrons to unoccupied valence orbitals as well as to the continuum, and its advantage is related to the localized character of core excitations, thus making K- and L-edge spectra sensitive to both the electronic structure and the local surroundings of the absorbing species. Cu(II) $L_{2,3}$ spectra are dominated by the electric dipole allowed 2p → 3d transitions, which provide information about the contribution of Cu 3d atomic orbitals (AOs) to the unoccupied molecular orbitals (MOs). In this regard, Solomon *et al.*[2] suggested the possible use of the intensity and position of the Cu(II) L_3 peak to get an experimental evaluation of the different degree of the Cu–ligands covalency as well as of the different ligand-field strengths, relative to some well-defined Cu(II) complex. Specifically, they focused on the Cu $L_{2,3}$ spectra of D_{2d}-$Cs_2[CuCl_4]$, D_{4h}-(N-mph)$_2[CuCl_4]$ (N-mph = N-methyl-N-phenethylammonium) and Cu(II) plastocyanin and, using D_{4h}-$[CuCl_4]^{2-}$ (**I**) as a reference, they assessed that the Cu–ligand interaction is more covalent in Cu(II) plastocyanin than in **I**. Since then, the simulation of $L_{2,3}$ spectra has represented a very dynamic line of work,[3-6] and the approach employed by Josefsson *et al.*,[4] which combines a high-level quantum chemical description of the chemical interactions and local atomic multiplet effects, is the actual state of art in this field.

As a part of a systematic investigation of the electronic properties of energy-targeted materials,[7] some of us have recently investigated the occupied and empty electronic structure of Cu(II) phthalocyanine (**II**, see Figure 1) by exploiting photoelectron spectroscopies and XAS at the C and N K-edge as well as at the Cu $L_{2,3}$-edges.[7b] The assignment of experimental evidences, collected for thick films of randomly oriented molecules, was guided by the results of ADF (Amsterdam Density Functional) calculations[8] and, besides the very good agreement between experiment and theory, the comparison between homogeneous theoretical results pertaining to the ground states of **I** and **II** emphasized the more ionic nature of the Cu–N interaction compared to the Cu–Cl one.[7b]

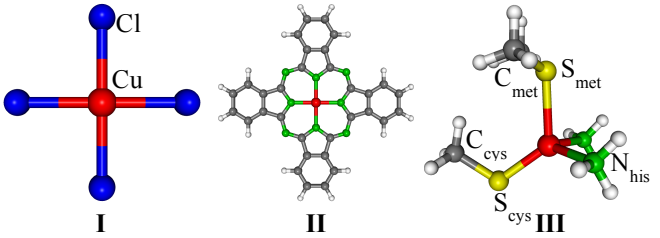

Fig. 1 Schematic representation of **I**, **II** and **III**. Each molecular species has a σ_h plane corresponding to the *xy* plane in the selected framework. The atom labelling of **III** is the same reported in ref. 9.

In this communication, we have tested the capability of the time-dependent (TD) DFT[10] within the Tamm-Dancoff approximation (TDA)[11] coupled to the relativistic two-component zeroth-order regular approximation (ZORA)[12] including spin-orbit (SO) effects, as implemented in the latest version of ADF,[8] to simulate the Cu(II) $L_{2,3}$ spectra of **I**, **II** and of the blue copper active site in plastocyanin (**III**, see Figure 1) in terms of their oscillator strength (*f*) distributions. A further aim of this study has been that of verifying the legitimacy of using the Cu(II) L_3-edge intensity and position to look into the Cu(II)–ligand symmetry-restricted covalency[13] and the ligand-field strength.

Cu(II) electric dipole allowed 2p → 3d transitions generate two $2p^5 3d^{10}$ final states with different total angular momentum. The most relevant feature of the Cu(II) $L_{2,3}$ spectra is then the presence of the L_3 (at ~930 eV) and L_2 (at ~950 eV) features, the former having an intensity approximately twice the one of the latter.[2,7b] The simulated *f* distributions of **I**, **II** and **III**$^{NOS/OS14}$ are displayed in Figure 2; the

left panel includes the *f* distributions in the 915 – 960 eV excitation energy (*EE*) range, while an expanded view of the 920 – 935 eV range is reported in the right panel.

Despite the comparison between experiment[2,7b] and theory confirms the well-known *EE* underestimation (~7 eV, see Table 1), ultimately due to the XC potential deficiencies,[6] the SO-ZORA TDDFT-TDA *f* spectra correctly reproduce the L_3 and L_2 relative positions as well as the corresponding relative intensities in **I** and **III**.[2]

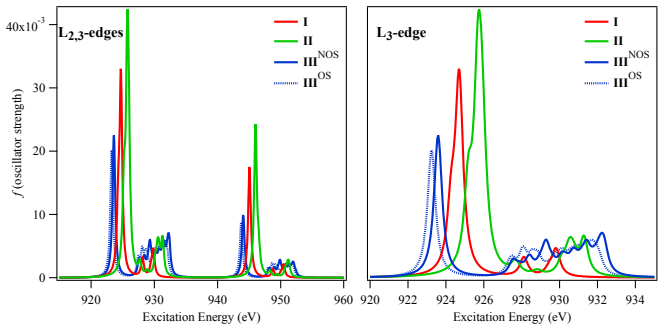

Fig. 2. SO-ZORA TDDFT-TDA Cu 2p excitation spectra of **I**, **II**, **III**$^{NOS/OS}$. Convoluted profiles are obtained with a Lorentzian broadening of 0.25 eV.[6b]

Nardi *et al.*[7b] ascribed the L_3 peak of **II** ($^{II}L_3$) to a single atom-like transition from the Cu $2p_{3/2}$ level to the $16b_{1g}$ spin-down (↓) lowest unoccupied MO (LUMO), significantly localized (52%) on the Cu-based $x^2 - y^2$ 3d AO. They also highlighted that the contribution of the same Cu-based AO to the $6b_{1g}$ LUMO(↓) of **I**, as obtained by homogeneous calculations, was significantly smaller (44%), thus indicating that the Cu–Cl interaction in **I** is more covalent than the Cu–N one in **II**. According to Solomon *et al.*,[2] this would imply, as actually found (see Figure 2), that *f* values associated to transitions generating $^{II}L_3$ should be larger than those corresponding to transitions generating $^{I}L_3$. Besides this intensity difference, a blue (red) shift of the L_3/L_2 peaks, when moving from **I** to **II** (**III**), and the presence of a shoulder on the lower *EE* side of $^{I}L_3$ and $^{II}L_3$ are well evident in the right panel of Figure 2. As far as the former point is concerned, Hocking and Solomon underlined that, in Cu(II) complexes, L_3-Δ*EE*s are mostly due to differences in the ligand-field strength, contemporarily emphasizing that the higher is the L_3-edge *EE*, the stronger is the ligand-field.[2b] Incidentally, neither the $^{III}L_3$ red shift[2] nor the $^{II}L_3$ blue shift[7b] relative to $^{I}L_3$ are unexpected. As a matter of fact, the weaker ligand field of **III** relative to **I** is related to the presence of only three (in **III**) rather than four (in **I**) equatorial ligands contributing to the destabilization of the Cu-based $x^2 - y^2$ 3d AO.[2b] Parallel arguments may be invoked to explain the $^{II}L_3$ blue shift, where both the different metal–ligand distances, shorter in **II** (1.968 Å) than in **I** (2.265 Å),[7b] and the ligand electronic properties (the presence of low lying empty π* MOs in the phthalocyanine ligand)[7b] concur to make the ligand-field in **II** stronger than in **I**.

Table 1. Experimental and theoretical excitation energies (eV) for the Cu 2p $L_{2,3}$ core excitation spectra of **I**, **II** and **III**$^{NOS/OS}$.

	I	**II**	**III**^{NOS}	**III**^{OS}
$^{exp}L_3$	931.0[2]	931.4[7b]	930.7[2]	
$^{exp}L_2$	951.0[2]	951.4[7b]	*a*	
L_3	924.67	925.75	923.60	923.24
L_2	945.06	946.00	944.07	943.71

[a]The energy of the $^{III}L_2$-edge is not reported in ref. 2.

Before addressing the $^{I}L_3$ and $^{II}L_3$ asymmetric shape, it has to be pointed out that the **III**^{NOS} *f* distribution numerically reproduces the L_3 red shift (1.0 eV) relative to **I**,[2] while the negative Δ*EE* is overestimated (1.4 eV) in **III**^{OS}. Despite such a result emphasizes the uselessness of a geometry optimization of **III** (see ESI), the comparison of SO-ZORA TDDFT-TDA results pertaining to **III**^{NOS} and **III**^{OS} is a gauge of the sensitivity of the adopted theoretical approach to identify even minor ligand-field strength variations. A final remark concerns the overestimation of the theoretical L_3 blue shift of **II** relative to **I**, ~ twice the one experimentally determined, which can be tentatively associated to the different methods and uncertainties in the calibration of Cu(II) $L_{2,3}$ spectra.[15]

As already mentioned, the lower *EE* sides of $^{I}L_3$ and $^{II}L_3$ are characterized by the presence of a shoulder. SO-ZORA TDDFT-TDA outcomes pertaining to **I**, **II**, and **III** and having the $2p_{3/2}$-based levels as initial spinors (IS) reveal that more than one excitation contribute to $^{X}L_3$ (**X** = **I**, **II**, **III**). Compositions and *f* values of transitions generating $^{X}L_3$ are reported in Table 2.[16]

Table 2. SO-ZORA TDDFT-TDA compositions[16] and $f \times 10^3$ values (in parentheses) of transitions generating $^{X}L_3^n$ excitations.[a,b,c,d,e,f,g]

	I	**II**	**III**^{NOS}
			$12a_{1/2} \rightarrow 108a_{1/2}^{(76)}$
L_3^1	$17a_{1/2} \rightarrow 100a_{1/2}^{(100)}$ (7.25)	$9a_{1/2} \rightarrow 294a_{1/2}^{(99)}$ (9.44)	$14a_{1/2} \rightarrow 108a_{1/2}^{(19)}$ (8.49)
			$13a_{1/2} \rightarrow 108a_{1/2}^{(4)}$
		$7a_{1/2} \rightarrow 294a_{1/2}^{(79)}$	$11a_{1/2} \rightarrow 108a_{1/2}^{(88)}$
L_3^2	$15a_{1/2} \rightarrow 100a_{1/2}^{(100)}$ (24.1)	$9a_{1/2} \rightarrow 295a_{1/2}^{(13)}$ (21.6)	$13a_{1/2} \rightarrow 108a_{1/2}^{(8)}$ (9.13)
		$10a_{1/2} \rightarrow 298a_{1/2}^{(8)}$	$14a_{1/2} \rightarrow 108a_{1/2}^{(3)}$
		$10a_{1/2} \rightarrow 298a_{1/2}^{(46)}$	
L_3^3		$9a_{1/2} \rightarrow 295a_{1/2}^{(33)}$ (12.1)	
		$7a_{1/2} \rightarrow 294a_{1/2}^{(20)}$	

[a]Contributions to IS → FS < 1% are not reported. [b]($f \times 10^3$) values < 5 are not reported. [c] $^{I}L_3^1$, $^{I}L_3^2$ *EE*s are 924.28 and 924.70 eV, respectively; $^{II}L_3^1$, $^{II}L_3^2$, $^{II}L_3^3$ *EE*s are 925.18, 925.69 and 925.90 eV, respectively; $^{III}L_3^1$, $^{III}L_3^2$ *EE*s are 923.57 and 923.60 eV, respectively. [d]Cu $2p_{3/2}$-based levels are: **I** ($15a_{1/2}$–$18a_{1/2}$, at 925.62, 925.57, 925.47, 925.46 eV), **II** ($7a_{1/2}$–$10a_{1/2}$, at 934.84, 934.76, 934.65, 934.65 eV), **III**^{NOS} ($11a_{1/2}$–$14a_{1/2}$, at 937.15, 937.14, 937.08, 937.08 eV).[16] [e]Parenthood of Cu $2p_{3/2}$-based levels with SR ZORA Cu 2p-based MOs is: **I** ($15a_{1/2} \rightarrow 2e_u^{(100)}$; $16a_{1/2} \rightarrow 2e_u^{(100)}$; $17a_{1/2} \rightarrow 1a_{2u}^{(67)} + 2e_u^{(33)}$; $18a_{1/2} \rightarrow 1a_{2u}^{(67)} + 2e_u^{(33)}$), **II** ($7a_{1/2} \rightarrow 1e_u^{(100)}$; $8a_{1/2} \rightarrow 1e_u^{(100)}$; $9a_{1/2} \rightarrow 1a_{2u}^{(67)} + 2e_u^{(33)}$; $10a_{1/2} \rightarrow 1a_{2u}^{(67)} + 2e_u^{(33)}$), **III** ($11a_{1/2} \rightarrow 5a''^{(60)} + 1a''^{(36)} + 6a'^{(4)}$; $12a_{1/2} \rightarrow 5a''^{(51)} + 1a''^{(49)}$; $13a_{1/2} \rightarrow 5a'^{(5)} + 1a''^{(32)} + 6a'^{(63)}$; $14a_{1/2} \rightarrow 5a'^{(17)} + 1a''^{(16)} + 6a'^{(67)}$). [f]Lowest unoccupied spinors of **I**, **II**, and **III** are the $100a_{1/2}$, $294a_{1/2}$, and $108a_{1/2}$ ones, respectively. [g]Parenthood of lowest unoccupied spinors of **I**, **II**, and **III** with SR ZORA LUMOs is: **I** ($100a_{1/2} \rightarrow 6b_{1g}^{(96)} + 5b_{1g}^{(3)}$), **II** ($294a_{1/2} \rightarrow 16b_{1g}^{(100)}$), **III** ($108a_{1/2} \rightarrow 18a''^{(93)} + 36a''^{(7)}$).

$^{III}L_3^1$ / $^{III}L_3^2$ and, separately, $^{III}f^1$ / $^{III}f^2$ values are very similar, thus explaining the absence of any shoulder in $^{III}L_3$. Moreover, all the transitions associated to $^{III}L_3$ have the same $108a_{1/2}$ final spinor (FS), strongly related (93%) to the scalar relativistic (SR) 18a″ LUMO, highly localized on the S_{cys} $3p_z$ (66%) and Cu $3d_{xz}$ (19%) AOs. Even though the 18a″ LUMO localization is quite different from that obtained by Penfield *et al.*[17] by means of spin-restricted self-consistent-field-Xα scattered-wave calculations (41 and 31% on S_{cys} 3p and Cu 3d AOs, respectively), results herein reported perfectly agree with those obtained by the Solomon group. As far as the ISs of transitions associated to $^{III}L_3$ are concerned, substantially all $2p_{3/2}$ Cu-based spinors participate to $^{III}L_3^1$ and $^{III}L_3^2$ (see Table 2). Differently from **III**, both $^{I}L_3^1$ and $^{I}L_3^2$ are generated by a single

transition having the same ($100a_{1/2}$) FS, strongly related (96%) to the SR $6b_{1g}$ LUMO of **I** having a 44% localization on the x^2 - y^2 3d AO. Interestingly, the $15a_{1/2}\rightarrow 100a_{1/2}$ transition, contrarily to the $17a_{1/2}\rightarrow 100a_{1/2}$ one, involves spinors having a parentage with SR MOs completely localized in the molecular plane. In addition, the ${}^{\mathbf{I}}L_3^2$ *EE* higher than the ${}^{\mathbf{I}}L_3^1$ one by 0.42 eV explains the shoulder on the lower *EE* side of ${}^{\mathbf{I}}L_3$.

Moving to the *f* distribution of **II**, SO-ZORA TDDFT-TDA results highlight the presence of three, rather than two, contributions to ${}^{\mathbf{II}}L_3$. Moreover, the corresponding *EE* spread (0.72 eV)[18] is larger than in **I** (0.42 eV), thus providing a rationale for the more evident asymmetry of the ${}^{\mathbf{II}}L_3$ feature. According to theoretical outcomes, ${}^{\mathbf{II}}L_3^1$ is assigned to the single $9a_{1/2}\rightarrow 294a_{1/2}$ transition whose FS is highly reminiscent (99%) of the SR $16b_{1g}$ LUMO of **II**. At variance to that, three different transitions contribute to ${}^{\mathbf{II}}L_3^2$; nevertheless, the main contribution (79%) comes from the $7a_{1/2}\rightarrow 294a_{1/2}$ one, which, similarly to **I**, involves spinors related with SR MOs completely localized in the molecular plane. Despite these similarities, ${}^{\mathbf{II}}L_3^3$ strikingly distinguishes **II** from **I** and **III**. In fact, among the ${}^{\mathbf{II}}L_3^3$ contributions, only the $7a_{1/2}\rightarrow 294a_{1/2}$ transition has a $2p_{3/2}$ AOs → $16b_{1g}$ LUMO character. In this regard, it is noteworthy that the four quasi degenerate $295a_{1/2} - 298a_{1/2}$ spinors correspond to the SR ligand-based $7e_g$ MO, quite close in energy to the $16b_{1g}$ LUMO (see Figure 7 of ref. 7b) and characterized by a very tiny participation of Cu 3d AOs.

Conclusions

Cu(II) $L_{2,3}$ spectra of **I**, **II** and **III** have been assigned by using the SO-ZORA TDDFT-TDA method implemented in the ADF package. Simulated *f* distributions along the investigated series properly reproduce relative intensities and positions. Moreover, the adopted approach confirms the legitimacy of using the Cu(II) L_3-edge position to get information about the ligand-field strength, contemporarily underlining the possibility of a Cu-ligand symmetry-restricted covalency underestimation when using the Cu(II) L_3-edge intensity as a gauge. Even though further validation is certainly needed, theoretical evidences herein reported indicate that the Cu(II) L_3-edge spectrum of **II** includes contributions that cannot be associated to Cu(II) $2p_{3/2}$ → 3d transitions. This would then suggest to use the Cu(II) L_3-edge intensity to get information about the Cu-ligand symmetry-restricted covalency with some caution because it might imply an underestimation (the higher the intensity, the lower the symmetry-restricted covalency) of such a contribution to the metal-ligand interaction. As far as the suitability of the SO-ZORA TDDFT-TDA method implemented in ADF to evaluate excitation energies for open-shell systems such as Cu(II) complexes in a spin-unrestricted TDDFT calculation including spin-orbit coupling is concerned, there is no doubt that further validations are needed; nevertheless, results herein reported are not only a successful application of the method to treat a particular chemical problem, but also a successful theory test for the SO-ZORA TDDFT-TDA.

Acknowledgment

This work was financially supported by the Italian Ministry of the University and Research (PRIN-2010BNZ3F2, project DESCARTES), and the University of Padova (CPDA134272/13, project S3MArTA). The Computational Chemistry Community of the University of Padova (C3P) at the Department of Chemical Sciences is also acknowledged for providing the computer facilities.

Notes and references

[a]Department of Chemical Sciences and INSTM, via Marzolo 1, 35131 Padova, Italy.
[b]Istituto dei Materiali per l'Elettronica ed il Magnetismo, Consiglio Nazionale delle Ricerche IMEM-CNR, Via alla Cascata 56/C – Povo, 38123 Trento, Italy.
[c]Institut für Physik, Humboldt-Universität zu Berlin, Newtonstrasse 15, 12489 Berlin, Germany.

Electronic Supplementary Information (ESI) available: Computational details. See DOI: 10.1039/c000000x/

1 A. Bianconi, in *X-ray Absorption; Principles, Applications, Techniques of EXAFS, SEXAFS and XANES*, D. C. Koningsberger and R Prins, Eds. John Wiley & Sons: New York 1988; pp. 573–662
2 (a) S. J. George, M. D. Lowery and E. I. Solomon, S. P. Cramer, *J. Am. Chem. Soc.* 1993, **115**, 2968; (b) R. K. Hocking and E. I. Solomon, *Struct. Bond.* 2012, **142**, 155.
3 E. C. Wasinger, F. M. F. de Groot, B. Hedman, K. O. Hodgson and E. I. Solomon, *J. Am. Chem. Soc.* 2003, **125**, 12894.
4 I. Josefsson, K. Kunnus, S. Schreck, A. Föhlisch, F. de Groot, P. Wernet and M. Odelius, *J. Phys. Chem. Lett.* 2012, **3**, 3565 and references therein.
5 M. Roemelt, D. Maganas, S. DeBeer and F. Neese, *J. Chem. Phys.* 2013, **138**, 204101.
6 (a) G. Fronzoni, M. Stener, P. Decleva, F. Wang, T. Ziegler, E. van Lenthe and E. J. Baerends, *Chem. Phys. Lett.* 2005, **416**, 56; (b) M. Casarin, P. Finetti, A. Vittadini, F. Wang and T. Ziegler, *J. Phys. Chem. A* 2007, **111**, 5270; (c) B. E. Van Kuiken, M. Valiev, S. L. Daifuku, C. Bannan, M. L. Strader, H. N. Cho, N. Huse, R. W. Schoenlein, N. Govind and M. Khalil, *J. Phys. Chem A* 2013, **117**, 4444.
7 (a) F. Sedona, M. Di Marino, D. Forrer, A. Vittadini, M. Casarin, A. Cossaro, L. Floreano, A. Verdini and M. Sambi, *Nat. Mater.* 2012, **11**, 970; (b) M. V. Nardi, F. Detto, L. Aversa, R. Verucchi, G. Salviati, S. Iannotta and M. Casarin, *Phys. Chem. Chem. Phys.* 2013, **15**, 12864-12881; (c) M. V. Nardi, R. Verucchi, L. Aversa, M. Casarin, A. Vittadini, N. Mahne, A. Giglia, N. Nannarone and S. Iannotta, *New J. Chem.* 2013, **37**, 1036; (d) M. V. Nardi, R. Verucchi, C. Corradi, M. Pola, M. Casarin, A. Vittadini and S. Iannotta, *Phys. Chem. Chem. Phys*. 2010, **12**, 871.
8 Amsterdam Density Functional (ADF) version 2013.01. http://www.scm.com.
9 S. E. Shadle, J E. Penner-Hahn, H. J. Schugar, B. Hedman, K. O. Hodgson and E. I. Solomon, *J. Am. Chem. Soc.* 1993, **115**, 767.
10 F. Wang, T. Ziegler, E. van Lenthe, S. van Gisbergen and E. J. Baerends, *J. Chem. Phys.* 2005, **122**, 204103.
11 S. Hirata and M. Head-Gordon, *Chem. Phys. Lett.* 1999, **314**, 291.
12 (a) E. van Lenthe, E. J. Baerends and J. G. Snijders, *J. Chem. Phys.* 1993, **99**, 4597; (b) E. van Lenthe, E. J. Baerends and J. G. Snijders, *J. Chem. Phys.* 1994, **101**, 9783; (c) E. van Lenthe, A. Ehlers and E. J. Baerends, *J. Chem. Phys.* 1999, **110**, 8943.
13 (a) C. K. Jørgensen, *Absorption Spectra and Chemical Bonding in Complexes*, Pergamon Press, Oxford, 1962.
14 NOS and OS acronyms stand for Non-Optimized- and Optimized-Structure, respectively (see ESI).

15 D_{4h}-(N-mph)$_2$[$CuCl_4$] and Cu(II) plastocyanin spectra were calibrated by taking as a reference the CuF_2 L_3 peak position (930.5 eV),[2a] while the $L_{2,3}$ CuPc spectrum was calibrated by referring to the $4f_{7/2}$ Au level (84.00 eV).[7b]

16 *EE* calculations have to be carried out with no symmetry. The spinor labelling is the one reported by P. W. M. Jacobs in *Group Theory With Applications in Chemical Physics*, Cambridge University Press, Cambridge, 2005, p. 450.

17 K. W. Penfield, A. A. Gewirth and E. I. Solomon, *J. Am. Chem. Soc.* 1985, **107**, 4519.

18 The experimental $^{II}L_3$ full width at half maximum is 1.3 eV.[7b]

A theoretical study of the L_3 pre-edge XAS in Cu(II) complexes

G. Mangione,[a] M. Sambi,[a] M. V. Nardi[b,c] and M. Casarin*[a]

$L_{2,3}$ spectra of Cu(II) complexes have been simulated by means of time dependent DFT. Besides the agreement between theory and experiment, the adopted approach provided further insights into the use of the Cu(II) L_3-edge intensity and position to investigate the Cu–ligand symmetry-restricted covalency and the ligand-field strength.

TOC GRAPHICS